FULL PAPER

ADVANCED
ENGINEERING
MATERIALS
www.aem-journal.com

Check for updates

Effect of Volume Fraction of Gradient Nanograined Layer on Low-Cycle Fatigue Behavior of Cu

Li-Jun Jing, Qing-Song Pan, and Lei Lu*

Low-cycle fatigue properties and cyclic behaviors of two pure Cu samples skinned with different volume fractions of gradient nanograined (GNG) layer are investigated under total strain-amplitude-controlled fatigue tests. Increasing the volume fraction of high-strength GNG layer can greatly elevate the cyclic stress amplitude of GNG/coarse grain (CG) Cu, compared with that of CG Cu fatigued at the same strain amplitude. Distinctly, it does not clearly influence the low-cycle fatigue life of GNG/CG samples with different GNG volume fractions, i.e., both exhibit comparable fatigue lives, even longer than their CG counterpart. Such enhanced low-cycle fatigue life is mainly due to the progressive homogenization of the gradient surface nanostructure, which effectively suppresses the surface roughening and fatigue cracking of the GNG/CG samples during cyclic straining.

1. Introduction

Extensive investigations over the past decades indicated that homogeneously refining the grain size of metals into ultrafine or nanometer scale can greatly increase the strength and the high-cycle fatigue endurance limit under stress control.[1–3] However, the corresponding ultrafine grained (UFG) and nanograined (NG) metals/alloys inevitably exhibit much shorter low-cycle fatigue lives in a total strain fatigue life diagram, compared with their coarse grained (CG) counterparts.[1] Moreover, a severe cyclic softening phenomenon (i.e., the stress amplitude rapidly decreases with increasing the number of cycles) is universally detected in UFG and NG metals, especially cyclically deformed at a large strain amplitude.[4–6] The observed inferior fatigue properties of UFG and NG metals are attributed to their unstable nanostructures with a high density of defects and high stored energies, to some extent.[1,4–6] In particular, severe strain localized cyclic deformation in the presence of macroscopically shear banding or abnormal grain coarsening obviously decreases the

L.-J. Jing, Dr. Q.-S. Pan, Prof. L. Lu
Shenyang National Laboratory for Materials Science, Institute of Metal Research
Chinese Academy of Sciences
Shenyang 110016, P. R. China
E-mail: llu@imr.ac.cn

L.-J. Jing
School of Materials Science and Engineering
University of Science and Technology of China
Hefei 230026, P. R. China

The ORCID identification number(s) for the author(s) of this article can be found under https://doi.org/10.1002/adem.201900554.

fatigue damage resistance of high-strength nanostructured metals, which greatly limits their prospects in engineering applications because of safety concerns.[1]

How to suppress the cyclic strain localization and improve the fatigue life of high-strength nanostructured metals/alloys is of great importance in the field of materials sciences.[1,7] Previous studies show that obvious enhancement in the low-cycle fatigue life can be achieved in bimodal metals with micron-sized grains randomly embedded in UFG matrix after an appropriate annealing treatment.[8,9] However, their cyclic plastic strains are primarily localized in micron-sized grains, causing early crack initiation and failure, which can be obviously evidenced by a much lower fatigue limit (comparable with that of CG counterparts).[9] Therefore, the cyclic plastic strain localization is still the inflexible characteristic of metallic materials with bimodal structure under cyclic loading, resulting in early cracking and inferior high-cycle fatigue properties.[9]

Recently, gradient nanograined (GNG) materials with the spatially graded distributed grain sizes from nanometer in the surface to micron scale in the core exhibit a synergetic enhancement of mechanical properties, such as high strength, considerable ductility,[10–12] excellent wear resistance,[13] and improved resistance to fatigue cracking.[14–18] For instance, by introducing a 65 μm thick GNG surface layer (accounting for a volume fraction of about 4.3%) on a CG Cu rod with a diameter of 6 mm, the measured fatigue limit of GNG/CG Cu at 10^7 cycles is 88 MPa, much higher than that of CG Cu (56 MPa).[17] Microstructural observations revealed that abnormal grain growth is initiated from the subsurface layer, which obviously retards the crack initiation and thus results in the enhanced stress-controlled fatigue properties of GNG/CG metals.[16,17] More importantly, the strain-controlled fatigue life of GNG/CG Cu even doubles that of the CG counterpart.[14] Such superior fatigue resistance under strain control originates from homogeneous grain coarsening of the initially graded microstructure and suppressed surface roughening of cyclically deformed GNG/CG Cu.[14]

Compared to conventional metals with a homogenous structure, the typical heterogeneous microstructure of GNG materials itself exhibits multiple microstructure parameters, such as volume fraction,[19,20] gradient order,[21] gradient magnitude of the GNG layer[22,23] and so on, which provide a large space to further tailor their overall mechanical properties. For example, with increasing the GNG volume fraction from 4.3% to 13%, the fatigue limit of GNG/CG Cu can be increased from 88 to

**ADVANCED
SCIENCE NEWS**

www.advancedsciencenews.com

**ADVANCED
ENGINEERING
MATERIALS**

www.aem-journal.com

98 MPa.[17] Structural analysis revealed that increasing the volume fraction of GNG layer can postpone the onset of abnormal grain coarsening in a deeper subsurface layer and its propagation period to the topmost surface.[17] However, whether the GNG volume fraction influences the strain-controlled low-cycle fatigue properties and cyclic deformation behaviors of GNG/CG metals remains an open question yet, due to the difficulty in preparing metals with different GNG volume fractions.

In this study, two Cu samples with different volume fractions, 4.3% and 13%, of GNG surface layer are controllably prepared by surface mechanical grinding treatment (SMGT).[24] The low-cycle fatigue properties (including cyclic stress response and fatigue life) and cyclic-deformation-induced microstructural evolutions are systematically investigated under total strain-amplitude-controlled fatigue tests. The effects of GNG volume fraction on the low-cycle fatigue properties and fatigue behaviors of Cu samples are also analyzed.

2. Experimental Section

2.1. Sample Preparation

As-received commercial-purity (99.98 wt% in purity) Cu rods were first annealed at 450 °C for 1 h to form fully equiaxed recrystallization grains with an average size of 21 μm, and then machined into dog-bone shaped samples with a gauge length of 12 mm and a gauge diameter of 6 mm. The gauge sections and arc transitions were processed by SMGT at cryogenic temperature (≈170 K) with liquid nitrogen. The SMGT processes were set to repeat 3 and 8 times to obtain two different volume fractions of the GNG surface layer on CG Cu samples. The estimated volume fractions of GNG layer (including both NG and UFG layers) in the whole cross-section for the 3 and 8 passes samples were 4.3% and 13%, which were referred to as GNG 4 and GNG 13, respectively, the same as the samples previously reported by Jing et al.[17] Both samples exhibited a smooth surface with a comparable small surface roughness R_a of ≈0.3 μm and without surface cracks.

2.2. Low-Cycle Fatigue Tests

Total strain-controlled symmetric tension-compression fatigue tests of GNG/CG and CG Cu samples were performed on an Instron 8874 testing machine at ambient temperature. Before fatigue tests, all samples were electrochemically polished to obtain a smooth surface for subsequent surface observations. A dynamic strain gauge extensometer with a gauge length of 10 mm and a very high strain resolution (smaller than 0.01%) was applied to accurately control and measure the cyclic strain during cyclic deformation. A triangle wave with a strain rate of $0.2\%\,\mathrm{s}^{-1}$ was used. For performing low-cycle fatigue tests, total strain amplitudes ($\Delta\varepsilon_t/2$) of 0.3%, 0.5%, and 0.55% (typically larger than that of the critical transition strain amplitude of GNG/CG Cu ≈0.29%,[14] separating the low-cycle and the high-cycle regimes) were chosen. The fatigue life of each sample is defined as the number of cycles at which the stress amplitude has decreased to 50% of its maximum value. The fatigue lives of both GNG 4 and GNG 13 at each strain amplitude were obtained

by averaging the data of three samples. The error bar is the mean ± standard deviation.

2.3. Microstructure Characterization

The longitudinal-sectional microstructures of GNG/CG Cu before and after fatigue-to-failure under $\Delta\varepsilon_t/2$ of 0.5% were characterized via FEI Nova NanoSEM 430 field-emission gun scanning electron microscope (SEM) with electron channel contrast imaging. Corresponding high-magnified microstructures were further investigated by FEI Tecnai F20 transmission electron microscope (TEM). Over 500 grains from numerous TEM images were measured to determine the average grain size in different depths of the GNG layer. The three-dimensional surface features of both GNG/CG and CG Cu fatigued to failure at $\Delta\varepsilon_t/2 = 0.5\%$ were investigated by Olympus LEXT OLS4100 confocal laser scanning microscope (CLSM).

2.4. Hardness Tests

Microhardness tests were performed on the longitudinal section of GNG/CG Cu samples in the as-SMGTed state and those fatigued to failure at $\Delta\varepsilon_t/2 = 0.5\%$ using a Mitutoyo MVK-H3 microhardness tester with a load of 5 g and a holding time of 10 s. The microhardness value at each depth of GNG/CG samples was obtained by averaging 10 measurements, whereas the error bar was the mean ± standard deviation. The distance between two neighbouring indents was 50 μm to avoid the overlapping effect.

3. Results

3.1. Microstructures and Hardness Distributions

After the SMGT process, a spatial gradient microstructure is formed in GNG 4 (**Figure 1**a): composed of NGs in the top 5 μm thick layer (Figure 1c), UFGs in a depth of 5 to 65 μm (Figure 1d), and deformed CG layer with a high density of irregular dislocation cells or tangles from 65 to 365 μm depth (Figure 1e) adherent on a deformation-free CG core below a depth of 365 μm. Most UFGs and NGs in the GNG layer (top 65 μm thick) are in the roughly equiaxed shape, separated by curved grain boundaries (GBs) and with a high density of dislocations (Figure 1c,d). No obvious crystallographic texture exists in the GNG layer, as revealed by the corresponding selected area electron diffraction (SAED) patterns inserted in Figure 1c,d, the same as previously reported by Jing et al.[17] Compared to GNG 4, as-SMGTed GNG 13 sample exhibits a similar gradient structure with identical morphologies (Figure 1b,f,h), but with a much thicker GNG layer (≈200 μm) and deformed CG layer (≈400 μm).

The average grain/cell size distributions along the depth from the graded surface to the CG core of GNG 4 and GNG 13 in the as-SMGTed state are measured and plotted in **Figure 2**a. Clearly, the grain sizes in both samples are spatially graded distributed, especially in the GNG layer. For instance, the average grain size of GNG 4 gradually increases from ≈60 nm in the top surface layer to ≈21 μm in the core. Compared to GNG 4, GNG 13 exhibits a relatively smaller grain size at the same depth from the top surface, agreeing well with Figure 1, due to undergoing a larger
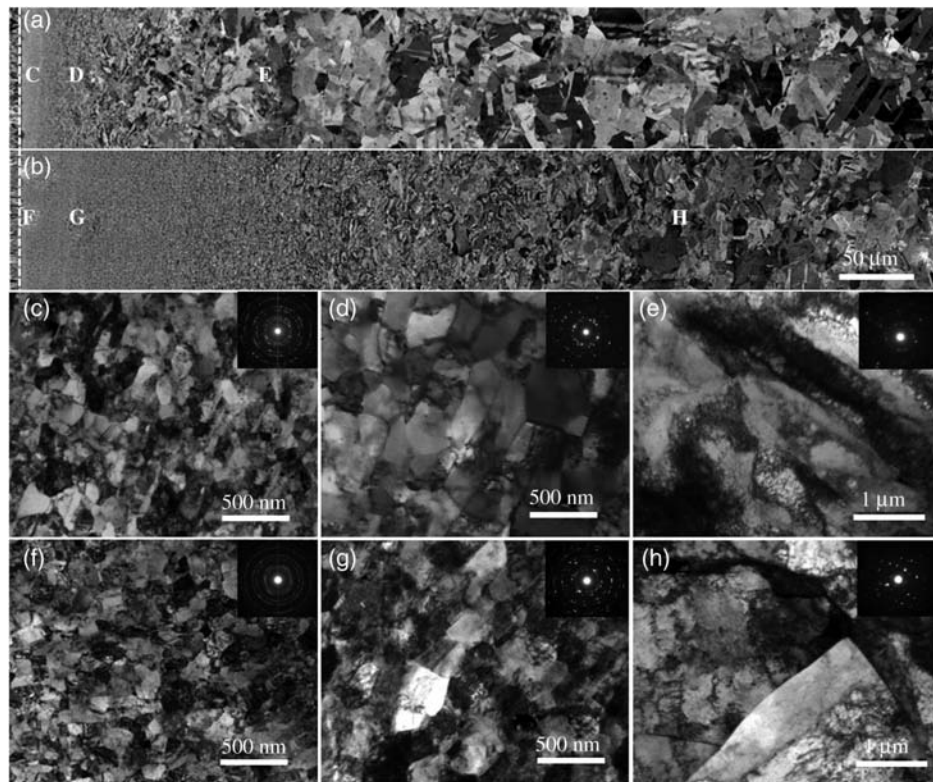
Figure 1. a) The typical longitudinal-sectional SEM images of GNG 4 and b) GNG 13. The dashed lines in (a,b) represent the treated surfaces. TEM images of microstructures (c–h) at positions C-H indicated in (a,b), respectively, and the insets in (c–h) are the SAED patterns.

accumulative plastic strain during SMGT processing. In particular, the mean grain size in the top surface layer of GNG 13 is reduced to ≈40 nm, about 20 nm smaller than that in GNG 4 sample.

The microhardness (H_V) distributions along the depth from the graded surface to the core of as-SMGTed GNG/CG samples are also measured and plotted in Figure 2b. Clearly, with the distance closer to the topmost surface for both GNG/CG samples, the measured Hv becomes larger, corresponding to the trend of decreased grain size in the GNG layer (Figure 2a). Note that the Hv data in the topmost 10 μm thickness (which should be highest due to the smallest grain size) are not measured, to avoid the influence of free surface on the indenter size (≈7 μm). In particular, a relatively higher microhardness is detected in the GNG surface layer of GNG 13, compared with GNG 4 at the same depth, which is consistent with its smaller grain size, as shown in Figure 2a. In contrast, the hardness in the strain-free CG cores below the 600 μm depth for both samples remains constant at ≈0.73 GPa (Figure 2b).

3.2. Strain-Controlled Fatigue Properties

Symmetric tension–compression fatigue tests under total strain control are performed on both GNG/CG samples. **Figure 3** shows the typical variations of cyclic stress–strain hysteresis loops for GNG 4, GNG 13, and CG Cu at a $\Delta\varepsilon_t/2$ of 0.5%. Compared with the flat hysteresis loop of CG Cu (Figure 3c),

the hysteresis loops of GNG 4 (Figure 3a) and GNG 13 (Figure 3b) are in a slim shape, especially at the initial number of fatigue cycles. In other words, the GNG/CG samples exhibit a higher peak stress than CG counterpart at the same fatigue condition, mainly due to the presence of high-strength GNG surface layer. For instance, the maximum stress of GNG 4 at the 2nd cycle is ≈135 MPa, much larger than that of CG Cu (77 MPa) (**Table 1**). A relatively larger peak stress (165 MPa) is detected in GNG 13 with a larger volume fraction of GNG layer. With increasing the number of cycles, the hysteresis loop of GNG 4 becomes slimmer with a gradually enhanced peak stress (Figure 3a), indicative of cyclic hardening. In contrast, the hysteresis loops of GNG 13 after 40 cycles nearly overlap with each other (Figure 3b), meaning that a cyclic stability is achieved.

The cyclic stress amplitude ($\Delta\sigma/2$) responses of GNG/CG Cu are shown in **Figure 4**. Due to the presence of high-strength GNG layer, the GNG/CG samples exhibit an elevated initial stress amplitude, compared with CG Cu at the same $\Delta\varepsilon_t/2$, consistent with that revealed by hysteresis loops shown in Figure 3. Taking the sample fatigued at a $\Delta\varepsilon_t/2$ of 0.5% as a typical instance, the $\Delta\sigma/2$ at the 2nd cycle is 135 and 165 MPa for GNG 4 and GNG 13, respectively, much larger than that of CG Cu (≈77 MPa) at the same cycle, indicating that introducing a GNG layer on a CG core can effectively increase the stress amplitude under strain control.

Two typical fatigue stages are found for both GNG 4 and GNG 13 in the whole fatigue life, according to the estimated hardening
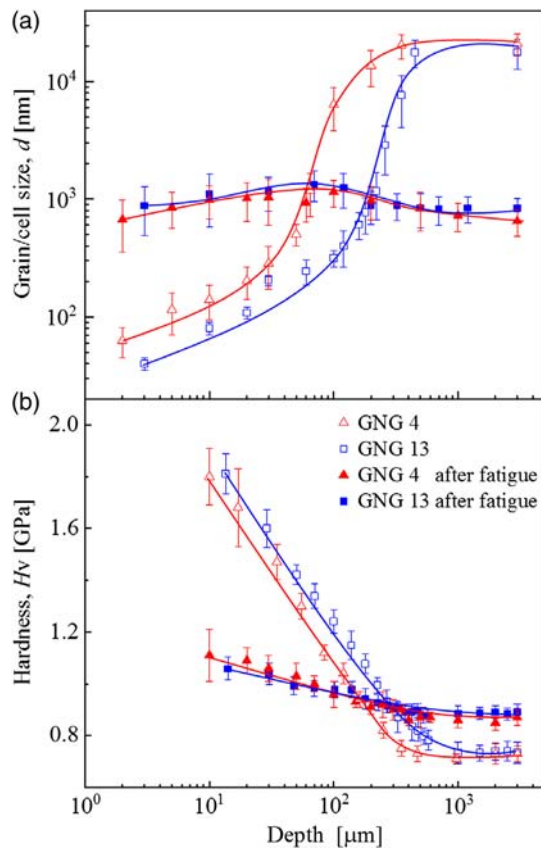
Figure 2. a) The variations of average grain/dislocation cell sizes and b) hardness along the depths from the topmost surface of GNG 4 and GNG 13 before and after fatigue-to-failure at $\Delta\varepsilon_t/2 = 0.5\%$.

rate (defined as the average stress increment per cycle, see details in Table 1). As shown in Figure 4, in the stage 1 (i.e., the initial 40 cycles, highlighted by the gray background regime), the stress amplitudes of both GNG/CG samples at a constant $\Delta\varepsilon_t/2$ increase rapidly with increasing cycles. The calculated hardening rate of GNG 4 at a $\Delta\varepsilon_t/2$ of 0.5% is $\approx$1.18 MPa cycle^{-1} and it decreases to $\approx$0.63 MPa cycle^{-1} for GNG 13; also both are smaller than that of CG counterpart (1.89 MPa cycle^{-1}) (Table 1). In contrast, in the stage 2 (after 40 cycles), the GNG/CG samples exhibit much smaller hardening rates than that observed in the stage 1. The estimated average hardening rate of GNG 4 at a $\Delta\varepsilon_t/2$ of 0.5% in the stage 2 is 3.4×10^{-3} MPa cycle^{-1}, more than two orders of magnitudes smaller than that in the stage 1. However, a cyclic stability with a nearly constant $\Delta\sigma/2$ is observed in GNG 13. With decreasing the strain amplitude to 0.3%, similar two fatigue stages are still detected in both GNG 4 and GNG 13. Most interestingly, the $\Delta\sigma/2$ of GNG 4 becomes almost the same as that of GNG 13 before failure for a given $\Delta\varepsilon_t/2$, although both samples have different volume fractions of GNG surface layer. The observed two-stages cyclic responses in GNG/CG samples, i.e., obvious cyclic hardening in the early stage of fatigue life followed by a slight cyclic hardening or stable stage in the later stage, are distinct from the typical continuous cyclic softening universally observed in various nanostructured metals/alloys prepared by means of severe plastic deformation.[1,5,6,25]
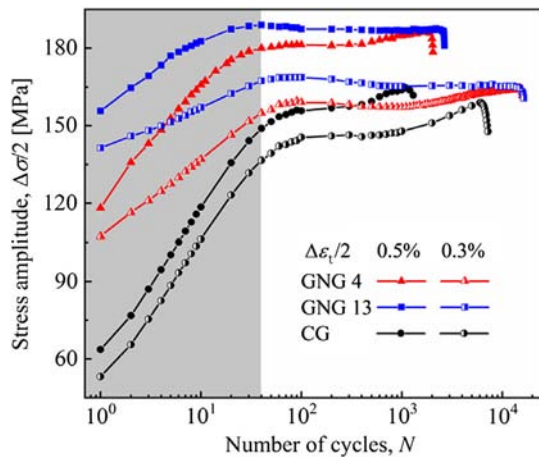
Total strain amplitude versus fatigue life curves in **Figure 5** show that the fatigue-to-failure life of GNG 4 under strain control is longer than that of CG counterpart, despite a slightly smaller uniform elongation for GNG 4.[17] The fatigue life of GNG 4 is $\approx$2.2 and 1.5 times than that of CG Cu at a $\Delta\varepsilon_t/2$ of 0.3% and 0.5%, respectively, far superior to UFG counterparts.[26] Most importantly, both GNG/CG samples exhibit a comparable fatigue
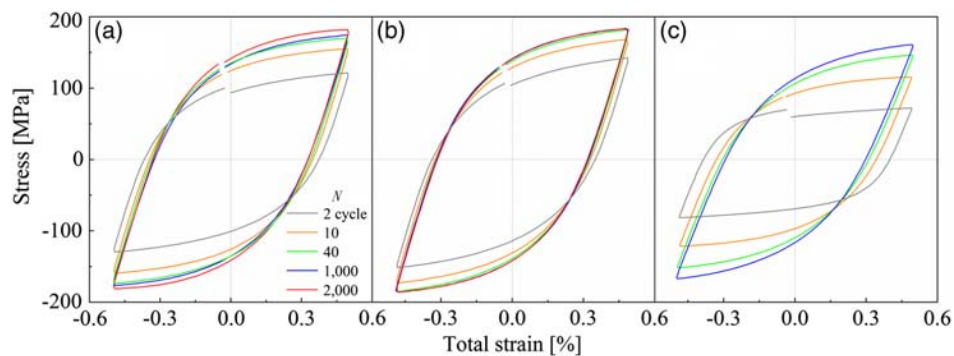

Figure 3. a) The developments of hysteresis loops of GNG 4, b) GNG 13, and c) CG Cu fatigued at $\Delta\varepsilon_t/2 = 0.5\%$, respectively.

Table 1. Stress amplitude and cyclic hardening rate of GNG 4, GNG 13, and CG Cu samples fatigued at $\Delta\varepsilon_t/2 = 0.3\%$ and 0.5%.

Total strain amplitude	0.3%					0.5%				
	Stress amplitude [MPa]			Hardening rate [MPa cycle^{-1}]		Stress amplitude [MPa]			Hardening rate [MPa cycle^{-1}]	
Number of cycles	2nd	40th	N_f	Stage 1	Stage 2	2nd	40th	N_f	Stage 1	Stage 2
GNG 4	116	155	166	1.03	6.7×10^{-4}	135	180	188	1.18	3.4×10^{-3}
GNG 13	146	166	166	0.55	0	165	188	188	0.63	0
CG	66	137	159	1.87	3.7×10^{-3}	77	149	165	1.89	1.7×10^{-2}

Figure 4. The cyclic stress responses of GNG 4, GNG 13, and CG Cu samples fatigued at $\Delta\varepsilon_t/2 = 0.5\%$ and 0.3%, respectively.
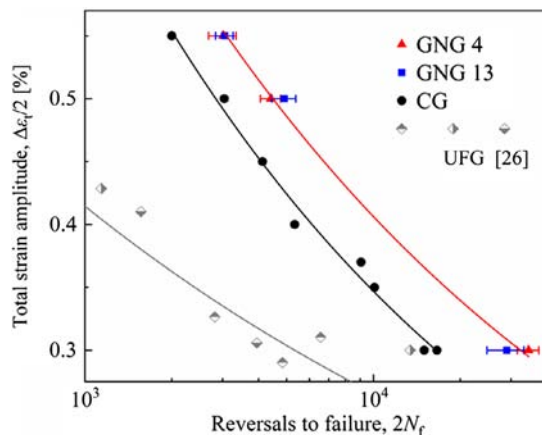
Figure 5. Dependence of the fatigue life on the strain amplitude of Cu samples under total strain control. The error bar is the mean ± standard deviation from three samples. Data of UFG Cu from the previous studies by Pan and Lu[26] are also included for comparison.

life at the same $\Delta\varepsilon_t/2$, indicating the volume fraction of the GNG layers does not clearly influence the low-cycle fatigue life of GNG/CG Cu under strain-controlled cyclic tests.

3.3. Microstructures after Fatigue-to-Failure

To elucidate the influence of the volume fraction of the GNG layer on the low-cycle fatigue behavior, the microstructures of GNG 4 and GNG 13 after fatigue-to-failure at a $\Delta\varepsilon_t/2$ of 0.5% are investigated by SEM and TEM. The original gradient nanostructures of both GNG 4 and GNG 13 are transformed to a relatively homogeneous microstructure after cyclic straining (**Figure 6**a,b), distinct from the strain-localized cyclic behavior such as shearing banding and/or abnormal grain coarsening in the fatigued UFG and NG metals.[27,28] Closer TEM observations reveal that homogeneous grain growth occurs in the original NG and UFG layer of GNG 4 and GNG 13 (Figure 6c,d,f,g) during cyclic loading. Most grains in

the GNG layer are separated by sharp GBs and are very clean with few intra-crystalline dislocations, whereas some dislocation debris are occasionally observed in several grains. In contrast, well-developed dislocation cells are detected in the original deformed CG layer and the CG interior of both GNG/CG samples after cyclic failure (Figure 6e,h), due to the accumulation and arrangement of dislocations during cyclic straining, similar to that observed in fatigued annealed CG structures.[29,30]
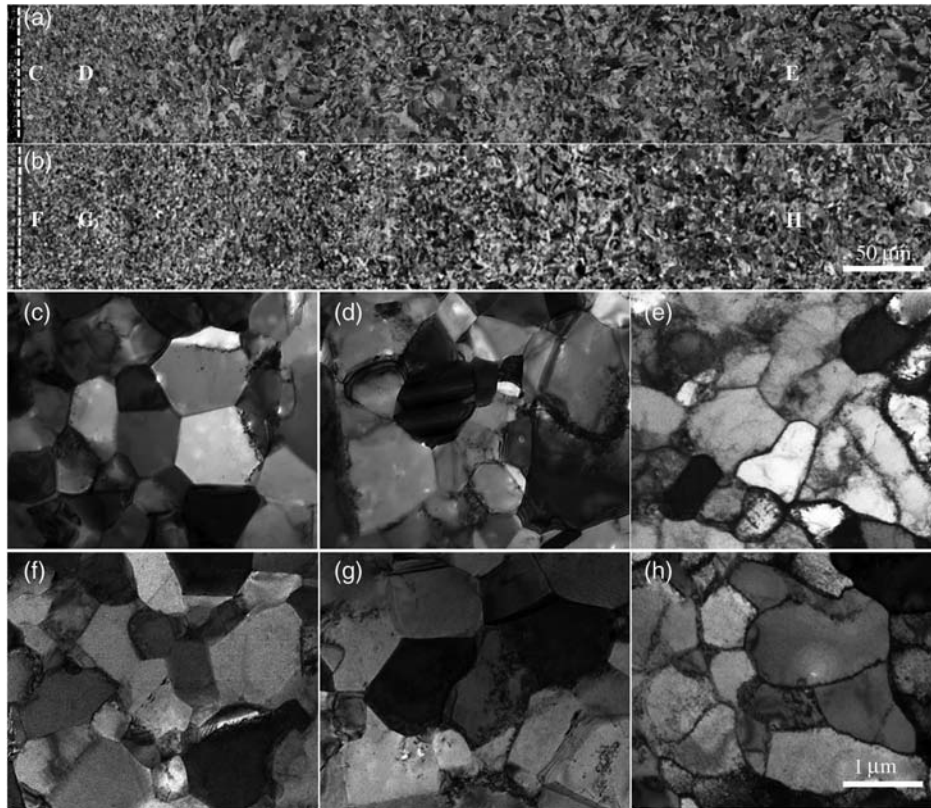
The statistical results in Figure 2a show that the average grain/cell size is almost homogeneously distributed in the whole cross-sections of GNG 4 and GNG 13 after large-amplitude cyclic straining. The measured coarsened grain sizes in the original NG and UFG layer for both GNG 4 and GNG 13 are 0.8 and 1 μm, respectively, which is roughly comparable with the refined cell size in the CG core (0.8 μm). Due to the pronounced grain coarsening in the GNG layer, an obvious drop of hardness occurs for GNG 4 and GNG 13 samples (Figure 2b). Interestingly, an overlapped hardness profile in the GNG layer of GNG 4 and GNG 13 is detected after cyclic deformation, although both exhibit different GNG volume fractions and initial hardness in the as-SMGTed state. For instance, the hardness of GNG 4 and GNG 13 has declined from ≈1.8 to ≈1.1 GPa at a depth of 10 μm. In contrast, a slight hardening from 0.73 to 0.89 GPa occurs in the CG interior of both samples due to the refinement effect of dislocation cells (Figure 6e,h). The Hv data in the whole cross-section of both GNG/CG samples are approximately comparable, further verifying a cyclic-straining-induced homogeneous structure (Figure 6).

4. Discussion

4.1. The Effect of GNG Volume Fraction on the Cyclic Response Behavior

The stress amplitude level of GNG/CG Cu under constant strain amplitude control is conjointly determined by the cyclic behaviors of the GNG surface layer and the CG core. The strength of GNG surface layer is much higher than that of CG core, due to the smaller grain size. The topmost 40 nm sized grains in GNG Cu exhibit a 10 times higher yield strength (≈660 MPa), relative to CG counterpart.[10] Furthermore, it has been verified that under a small-amplitude cyclic loading, the high-strength GNG layer mainly deforms elastically in the initial cycles (i.e., stage 1 in this study).[14] Hence, the presence of the high-strength GNG surface layer can obviously enhance the cyclic stress amplitude of GNG/CG sample, as shown in Figure 4. With increasing the volume fraction of GNG layer from 4.3% to 13%, the stress amplitude of GNG/CG Cu can be further improved. Despite accounting for a very limited volume fraction, the estimated contributions of the GNG layer to the stress amplitude of GNG 4 and GNG 13 at the 2nd cycle under $\Delta\varepsilon_t/2 = 0.5\%$ are 66 and 103 MPa, up to ≈49% and 62% of their own stress amplitudes, respectively, demonstrating a strong effect of GNG volume fraction on the cyclic stress amplitude of GNG/CG Cu.

The cyclic hardening rate of GNG/CG Cu is strongly influenced by the volume fraction of CG core. The cyclic hardening of GNG 4 and GNG 13 is mainly contributed by the dislocation accumulations and formation of dislocation cells induced hardening in the

ADVANCED
SCIENCE NEWS
www.advancedsciencenews.com

ADVANCED
ENGINEERING
MATERIALS
www.aem-journal.com

Figure 6. a) The typical longitudinal-sectional SEM images of GNG 4 and b) GNG 13 cyclically deformed to failure at $\Delta\varepsilon_t/2 = 0.5\%$. c–h) The typical TEM images of microstructures at positions C-H indicated in (a,b), respectively.

CG core. With increasing the GNG volume fraction, the decreased volume fraction of the hardenable CG core (from 90% to 81% shown in Figure 2b) reduces the hardening rate of GNG/CG samples accordingly, especially in the stage 1. The measured hardening rate of GNG 4 and GNG 13 in the stage 1 is ≈0.6 and 0.3 times than that of CG Cu, respectively (Table 1). With increasing the number of cycles (in the stage 2), grain-coarsening-induced softening in the GNG layer further reduces the hardening rate of GNG/CG samples. The measured hardening rate of GNG 4 in the stage 2 at the strain amplitude of 0.3% and 0.5% is only one-fifth of that of CG Cu (Table 1). Coincidentally, when the GNG volume fraction increases to 13%, the hardening from the CG interior is completely offset by the softening from the GNG layer, resulting in a cyclic stability of GNG 13 with almost zero hardening rate. Due to the slow but non-negligible cyclic hardening, the stress levels of GNG 4 at the strain amplitude of 0.3% and 0.5% are gradually increased to 166 and 188 MPa, respectively, comparable with that of GNG 13 before failure, which is consistent with similar homogeneous distributed microstructures and hardness between both samples (Figure 2 and 6).

4.2. The Effect of GNG Volume Fraction on the Surface Damage

The typical surface fatigue morphologies of both GNG 4 and GNG 13 at a $\Delta\varepsilon_t/2$ of 0.5% are investigated by SEM and CLSM, respectively. The SEM observations in **Figure 7**a reveal that the GNG 4 sample still exhibits a relatively smooth surface even fatigued-to-failure, with only a few damage features. The CLSM observations in Figure 7b,c show that the surface fluctuation in fatigued GNG 4 is ≈0.16 μm, an order of magnitude smaller than the micro-scale surface extrusions/intrusions (≈1.7 μm) of CG Cu (Figure 7g–i) induced by dislocation activities and deformation incompatibility of adjacent large-sized CGs.[31] These results indicate that surface roughening of cyclically deformed GNG 4 is effectively suppressed by the GNG surface layer. Compared with GNG 4, the surface of GNG 13 sample after fatigue seems mildly smoother, with less number of surface fluctuations (Figure 7d,e). The measured maximum surface fluctuation in GNG 13 is ≈0.12 μm (Figure 7f), almost comparable with that in GNG 4, indicating that the volume fraction of GNG layer exhibits a minor influence on surface damage during cyclic loading.

The suppressed surface roughening of GNG 4 and GNG 13 is mainly determined by the following two factors: 1) The progressive homogenization of GNG layer via orderly cyclic plastic strain transmission from the CG core to the GNG layer of both samples can effectively suppress strain localization in the conventional samples with homogeneous CG and nanostructures.[14] Furthermore, during the process of grain coarsening, the initial high-density defects (including dislocations and GBs, which usually act as stress concentrators) in the GNG surface layer can be swept off, analogous to the cyclic deformation-induced defect
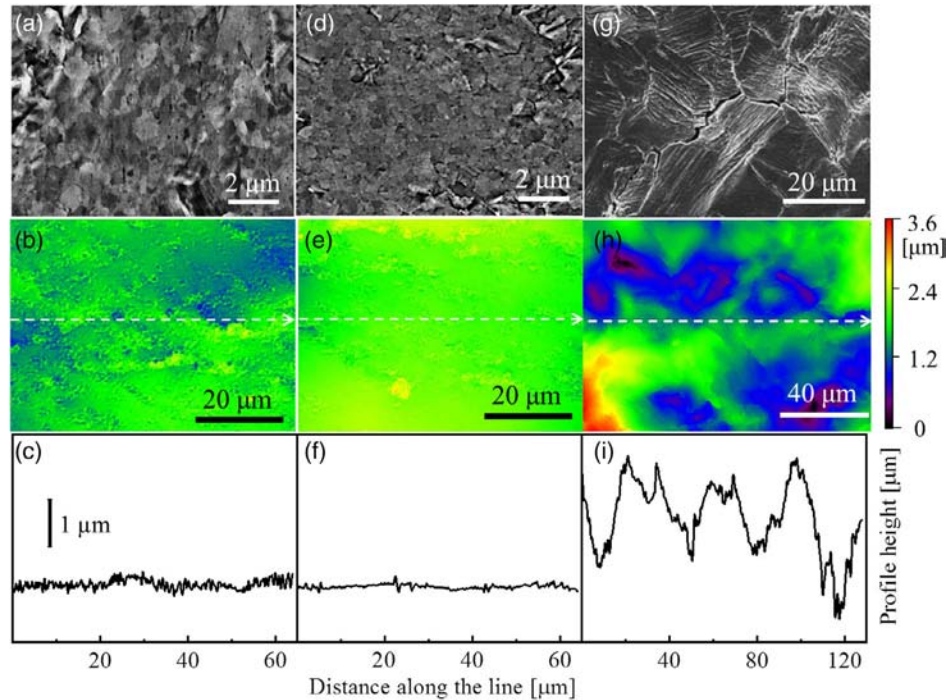
Figure 7. a,d,g) The top-view SEM, b,e,h) CLSM images, and c,f,i) surface fluctuations of a–c) GNG 4, d–f) GNG 13, and g–i) CG after fatigue-to-failure at $\Delta\varepsilon_t/2 = 0.5\%$. The "hill" and "valley" profiles (c,f,i) along the dashed arrows in (b,e,h), respectively.

healing in submicron-sized Al single crystal.[32] 2) Due to a relatively small coarsened grain size of ≈0.8 μm after fatigue-to-failure, the conventional rough dislocation patterns with the characteristic structural dimensions typically much larger than or at least comparable to 1 μm cannot be formed. Both GNG/CG samples exhibit the same homogeneous grain-coarsening behavior and coarsened grain size (i.e., strain-delocalized cyclic deformation mechanism and microstructure evolutions), so the identical surface damage is understandable.

4.3. The Effect of GNG Volume Fraction on the Fatigue Life

The strain-controlled fatigue lives of metals with homogeneous microstructures are usually dominated by their tensile ductility, following the Coffin-Manson equation[30]

$$\frac{\Delta\varepsilon_p}{2} = \varepsilon_f'(2N_f)^c \tag{1}$$

Where $\frac{\Delta\varepsilon_p}{2}$ is the plastic strain amplitude, ε_f' is the fatigue plasticity coefficient which is related to the tensile ductility, N_f is the fatigue life, and c is the fatigue plasticity exponent. A better tensile ductility usually results in a longer fatigue life at a constant strain amplitude, as verified by the fatigue data of CG and UFG metals[1] and bimodal structured metals with CG embedded in UFG matrix.[9] In this study, although the uniform elongations of both GNG/CG Cu with different volume fractions of GNG layer are slightly smaller than that of CG counterpart,[17] both GNG/CG samples exhibit superior fatigue lives. This is mainly because the presence of a thin GNG surface layer can effectively suppress strain localization and surface roughness, which are universally detected in conventional homogeneous or bimodal structures, thus retarding fatigue cracking and early failure. The identical strain-delocalized cyclic deformation mechanism, similar microstructure evolution processes (Figure 6) and surface damage of both GNG/CG samples (Figure 7) result in a comparable strain-controlled fatigue life, irrespective of the volume fraction of the GNG layer.

Previous study has shown that with increasing the GNG volume fraction from 4.3% to 13%, the fatigue limit of GNG/CG Cu increases from 88 to 98 MPa.[17] Combining with the present results, it can be concluded that the superior all-round fatigue performance with longer fatigue life in low-cycle regime and enhanced fatigue endurance limits in high-cycle regime can be achieved in GNG/CG metals, distinct from the trend of trade-off of high-cycle and low-cycle fatigue properties for conventional metals with homogeneous nanostructures, i.e., a high fatigue limit but a much shortened fatigue life.[1,7]

The process of SMGT, like other surface treatment methods, such as deep rolling and shot peening,[33–36] can also induce a residual compressive stress in the GNG surface layer, due to an inhomogeneous plastic deformation in grains or between grains.[36] Previous study indicated that residual stress can improve the high-cycle fatigue life of GNG/CG Cu due to the suppressed initiation and propagation of cracks in the tension side.[36] However, a few studies have demonstrated large-amplitude cyclic straining in low-cycle fatigue tests will induce microstructure recovery/grain coarsening and the rapid release of residual stress in the GNG layer in very short initial cycles.[15,33,37] For instance, the residual stresses of gradient nanostructured 316L stainless steel can be rapidly released after

fatigue to only $6\% N_f$ at $\Delta \varepsilon_t/2 = 0.4\%$.[15] From this point of view, the influences of compressive stress on alleviating surface roughening and improving low-cycle fatigue life of GNG metals will be negligible. For GNG/CG Cu in this study, the influence of homogeneous grain coarsening of GNG under low-cycle fatigue on the residual compressive stress should be studied further to understand the effect of the residual compressive stress on the low-cycle fatigue life of GNG/CG Cu.

5. Conclusion

Strain-controlled low-cycle fatigue tests of GNG/CG Cu with different volume fractions of GNG surface layer reveal that increasing the volume fraction of GNG layer can obviously enhance the cyclic-stress amplitude of GNG/CG Cu but almost not sacrifice the low-cycle fatigue lifetime, instead which are comparable and superior to the CG counterpart. Homogeneous grain coarsening, associated with identical microstructure homogenization and suppressed surface roughness, occurs in both samples during the large-amplitude cyclic straining, irrespective of the GNG volume fraction, thus contributing to the comparable enhanced low-cycle fatigue lives. Our finding points out a simple strategy for enhancing fatigue resistance of engineering components via tailor-designing a thin GNG skin on a CG substrate.

Conflict of Interest

The authors declare no conflict of interest.

[1] H. Mughrabi, H. W. Höppel, *Int. J. Fatigue* **2010**, *329*, 1413.
[2] T. Hanlon, Y.-N. Kwon, S. Suresh, *Scripta Mater.* **2003**, *497*, 675.
[3] L. Kunz, P. Lukáš, M. Svoboda, *Mater. Sci. Eng. A* **2006**, *4241–2*, 97.
[4] A. Vinogradov, S. Hashimoto, *Mater. Trans.* **2001**, *421*, 74.
[5] S. R. Agnew, J. R. Weertman, *Mater. Sci. Eng. A* **1998**, *2442*, 145.
[6] H. W. Höppel, Z. M. Zhou, H. Mughrabi, R. Z. Valiev, *Philos. Mag. A* **2002**, *829*, 1781.
[7] A. Pineau, A. A. Benzerga, T. Pardoen, *Acta Mater.* **2016**, *107*, 508.
[8] H. W. Höppel, R. Z. Valiev, *Z. Metallkd.* **2002**, *937*, 641.
[9] M. Korn, R. Lapovok, A. Böhner, H. W. Höppel, H. Mughrabi, *Kovove Mater.* **2011**, *49*, 51.
[10] T. H. Fang, W. L. Li, N. R. Tao, K. Lu, *Science* **2011**, *3316024*, 1587.
[11] Y. J. Wei, Y. Q. Li, L. C. Zhu, Y. Liu, X. Q. Lei, G. Wang, Y. X. Wu, Z. L. Mi, J. B. Liu, H. T. Wang, H. J. Gao, *Nat. Commun.* **2014**, *5*, 3580.
[12] X. L. Wu, P. Jiang, L. Chen, F. P. Yuan, Y. T. Zhu, *Proc. Natl. Acad. Sci.* **2014**, *11120*, 7197.
[13] X. Chen, Z. Han, X. Y. Li, K. Lu, *Sci. Adv.* **2016**, *212*, e1601942.
[14] J. Z. Long, Q. S. Pan, N. R. Tao, M. Dao, S. Suresh, L. Lu, *Acta Mater.* **2018**, *166*, 56.
[15] Y. B. Lei, Z. B. Wang, J. L. Xu, K. Lu, *Acta Mater.* **2019**, *168*, 133.
[16] L. Yang, N. R. Tao, K. Lu, L. Lu, *Scripta Mater.* **2013**, *6810*, 801.
[17] L. J. Jing, Q. S. Pan, J. Z. Long, N. R. Tao, L. Lu, *Scripta Mater.* **2019**, *161*, 74.
[18] J. Z. Long, Q. S. Pan, N. R. Tao, L. Lu, *Scripta Mater.* **2018**, *145*, 99.
[19] X. C. Yang, X. L. Ma, J. Moering, H. Zhou, W. Wang, Y. L. Gong, J. M. Tao, Y. T. Zhu, X. K. Zhu, *Mater. Sci. Eng. A* **2015**, *645*, 280.
[20] J. Li, A. K. Soh, *Int. J. Plast.* **2012**, *39*, 88.
[21] Z. W. Ma, J. B. Liu, G. Wang, H. T. Wang, Y. J. Wei, H. J. Gao, *Sci. Rep.* **2016**, *6*, 22156.
[22] Y. Lin, J. Pan, H. F. Zhou, H. J. Gao, Y. Li, *Acta Mater.* **2018**, *153*, 279.
[23] X. J. Yang, J. X. Zhou, X. Ling, *Mater. Des.* **2013**, *43*, 454.
[24] W. L. Li, N. R. Tao, K. Lu, *Scripta Mater.* **2008**, *595*, 546.
[25] Z. J. Zhang, P. Zhang, Z. F. Zhang, *Acta Mater.* **2016**, *121*, 331.
[26] Q. S. Pan, L. Lu, *Acta Mater.* **2014**, *81*, 248.
[27] S. Malekjani, P. D. Hodgson, N. E. Stanford, T. B. Hilditch, *Scripta Mater.* **2013**, *6810*, 821.
[28] S. D. Wu, Z. G. Wang, C. B. Jiang, G. Y. Li, I. V. Alexandrov, R. Z. Valiev, *Scripta Mater.* **2003**, *4812*, 1605.
[29] P. Lukáš, M. Klesnil, *Mater. Sci. Eng.* **1973**, *116*, 345.
[30] S. Suresh, *Fatigue of Materials*, 2nd ed., Cambridge University Press, Cambridge, UK **1998**.
[31] W. H. Kim, C. Laird, *Acta Metall.* **1978**, *265*, 777.
[32] Z. J. Wang, Q. J. Li, Y. N. Cui, Z. L. Liu, E. Ma, J. Li, J. Sun, Z. Zhuang, M. Dao, Z. W. Shan, S. Suresh, *Proc. Natl. Acad. Sci.* **2015**, *11244*, 13502.
[33] K. Dalaei, B. Karlsson, L. E. Svensson, *Mater. Sci. Eng. A* **2011**, *5283*, 1008.
[34] C. Ye, A. Telang, A. S. Gill, S. Suslov, Y. Idell, K. Zweiacker, J. M. K. Wiezorek, Z. Zhou, D. Qian, S. R. Mannava, V. K. Vasudevan, *Mater. Sci. Eng. A* **2014**, *613*, 274.
[35] R. K. Nalla, I. Altenberger, U. Noster, G. Y. Liu, B. Scholtes, R. O. Ritchie, *Mater. Sci. Eng. A* **2003**, *3551*, 216.
[36] J. Z. Long, Q. S. Pan, N. R. Tao, L. Lu, *Mater. Res. Lett.* **2018**, *68*, 456.
[37] Q. Wang, X. S. Liu, Z. J. Yan, Z. B. Dong, D. J. Yan, *Int. J. Fatigue* **2017**, *105*, 43.